Supplementary Information (SI) for Journal of Materials Chemistry B.
This journal is © The Royal Society of Chemistry 2024

Supplementary Information

Self-Assembled Copper-Artemisinin Nanoprodrug as an Efficient Reactive Oxygen Species Amplified Cascade System for Cancer Treatment

Xueyu Zhu,[+] Chenyang Bi,[+] Wei Cao,[+] Shuangshuang Li, Chuting Yuan, Pengping Xu, Dongdong Wang, Qianwang Chen,* and Lei Zhang**

X. Zhu, W. Cao, S. Li, Prof. L. Zhang

Institute of Clinical Pharmacology, Anhui Medical University, Hefei, 230032, China; Department of Pharmacy, The First Affiliated Hospital of USTC, Division of Life Sciences and Medicine, University of Science and Technology of China, Hefei, 230001, China; Anhui Provincial Key Laboratory of Precision Pharmaceutical Preparations and Clinical Pharmacy, Hefei, 230001, China

E-mail: zhanglei6@ustc.edu.cn

C. Bi, C. Yuan, P. Xu, Prof. D. Wang, Prof. Q. Chen

Hefei National Laboratory for Physical Sciences at Microscale, Department of Materials Science & Engineering & Collaborative Innovation Center of Suzhou Nano Science and Technology, CAS High Magnetic Field Laboratory, University of Science and Technology of China, Hefei, 230026, China

E-mail: wangdd13@ustc.edu.cn; cqw@ustc.edu.cn

[+] These authors contributed equally to this work.

Keywords: self-assemble • bio-inspired nanoprodrug • artemisinin • chemodynamic therapy • copper ions

Reagents and materials: Artesunate, fluorescein diacetate (FDA), propidium iodide (PI), and anhydrous copper chloride ($CuCl_2$) were form Shanghai Aladdin Biochemical Technology Co., Ltd; Acetic acid (HPLC) was from Fisher. Histidine, hydrochloric acid (HCl), sodium hydroxide (NaOH), methanol and acetonitrile (HPLC) were form Sinopharm Chemical Reagent Co., Ltd.; HEPES (4-(2-hydroxyethyl)-1-piperazineethanesulfonic acid) was purchased from Sigma-Aldrich; Tris buffer, D-Luciferin potassium salt (4,5-dihydro-2-(6-hydroxy-2-benzothiazolyl)-4S-thiazolecarboxylic acid, and monopotassium salt) were from Shanghai Sangon. Reactive Oxygen Species Assay Kit (DCFH-DA, S0033), GSH and GSSG Assay Kit (S0053), Cell Counting Kit-8 (C0037) and Annexin V-FITC Apoptosis Detection Kit (C1062S) were from Beyotime; Dulbecco's Modified Eagle Media (DMEM) was from Gibco; Ready-to-use dialysis device (Tube-O-DIALYZER™, Medi) was from G-Biosciences. All chemicals were used as received unless otherwise stated.

Cell lines: murine breast cancer cells (4T1) were cultured in the DMEM medium supplemented with 10% FBS, 100 U mL^{-1} penicillin and 100 μg mL^{-1} streptomycin under a humid atmosphere at 37 ℃ and 5% CO_2.

Measurements: The structure of artesunate-histidine was characterized by a JNM-ECZ600R Nuclear Magnetic Resonance Spectroscopy with TMS as the internal standard. The ESI-MS spectrum were recorded using an LTQ-Orbitrap XL Electrostatic Field Orbital Trap Mass Spectrometer. The nanoprodrug was characterized by a transmission electron

microscope (JEOL JEM-2100F) with an accelerating voltage of 200 kV. Supra 40 (Zeiss, Netherlands) with 5 kV accelerating voltage was used for scanning electron microscopy (SEM) measurements. Ultraviolet-visible (UV-vis) absorption spectra were measured with a Persee TU-1810. The hydrodynamic size and zeta potential were measured at 25 °C with a Malvern Zetasizer. UPLC measurements were performed on the ACQUITY UPLC H-Class system equiped with a BEH HILIC 1.7 μm chromatographic column (Waters).

Synthesis of AH: Artesunate (2.0 g,5.2 mmol), DCC (1.18 g,5.7 mmol) and NHS (658 mg,5.7 mmol) were mixed together in dichloromethane. After stirring in an ice bath for 12 h, the reaction mixture was filtered. The solvent was subsequently removed by rotary evaporation.Next, solid white powder was obtained via flash column chromatography (silica, pure ethyl acetate as the eluent). Later, the obtained intermediate was dissolved in DMF. Histidine (968 mg,6.2 mmol) in H_2O was then added into the mixture. After stirring in an ice bath for an additional 12 h, the mixture was evaporated under reduced pressure to yield pure artesunate-histidine conjugate as a white solid (624 mg,30 %). 1H NMR (600 MHz, DMSO-d6) δ 8.16 (d, J = 7.7 Hz, 1H), 7.57 (d, J = 29.4 Hz, 1H), 6.83 (d, J = 50.1 Hz, 1H), 5.64 (d, J = 9.8 Hz, 1H), 4.37 (td, J = 7.8, 5.4 Hz, 1H), 2.91 (dd, J = 14.8, 5.6 Hz, 1H), 2.81 (dd, J = 14.8, 8.0 Hz, 1H), 2.54 (dd, J = 11.8, 6.2 Hz, 1H), 2.42 (t, J = 6.9 Hz, 1H), 2.32 – 2.22 (m, 2H), 2.18 (td, J = 14.0, 3.9 Hz, 1H), 1.99 (dt, J = 14.6, 3.8 Hz, 1H), 1.81 (ddt, J = 13.6, 6.9, 3.6 Hz, 1H), 1.61 (td, J = 14.2, 13.7, 3.5 Hz, 2H), 1.53 (t, J = 4.4 Hz, 1H), 1.44 (dt, J = 13.0, 6.0 Hz, 1H), 1.28 (s, 3H), 1.17 (td, J = 11.4, 6.6 Hz, 1H), 1.01 – 0.90 (m, 1H), 0.88 (d, J = 6.4 Hz, 3H), 0.75 (d, J = 7.1 Hz, 3H).

Synthesis of AHCu: 2 mg AH was dissolved in 100 μL HCl (50 mM) to get a transparent solution, followed by 780 μL ultrapure water and 100 μL $CuCl_2$ (10 mM) aqueous solution. The mixture was shaken for 5 minutes to homogenize the reagents. Finally, 20 μL of HEPES buffer (1.0 M, pH 7.6) was slowly added to the above mixture to obtain a white emulsion in an ultrasonic water bath. The product was centrifuged at 12,000 rpm for 5 minutes and the precipitate was washed with ultrapure water. Parallel trials were carried out (1 / 2 / 4 mg AH vs 1 mM $CuCl_2$ and 2 mg AH vs 0.5 / 1.0 / 2.0 mM $CuCl_2$) to determine the optimal molar ratio of reaction.

Stability of AHCu: The AHCu nanoprodrug in PBS were incubated at 4 ^{o}C. Dynamic light scattering was used to characterize particle size changes after incubation for extended period of time. The turbidity of the AHCu in water was also recorded by measuring the changes in absorption intensity at the wavelength of 600 nm.

Release profiles (pH responsive release of drug): The amide bond of artesunate and histidine was achieved by DCC/NHS reaction. After introducing copper ions, AHCu is synthesized by self-assembly driven by coordination. [1] 2 mg of AHCu was dispersed in 2 mL of water and then added to a ready-to-use dialysis tube (Tube-O-DIALYZER^{TM}, Medi). The dialysis tubing was then placed in a 10 mL buffer solutionn (pH 5.4 and 7.4). 100 μL of external solution is aspirated, filtered, and submitted to UPLC analysis at selected time intervals.

Depletion of GSH: Ellman's assay was employed to detect the depletion of GSH by the nanoparticle. 500 μL of AHCu solutions with different concentrations were mixed with 500 μL of 2 mM GSH solution and co-incubated 30 min at 37 °C. The positive control was 10 mM GSH. Then 1mL of PBS (pH = 7.4) solution and 10 μL of DTNB (3 $mg \cdot mL^{-1}$, DMSO) were added into the supernatant. The absorbance of the mixture at 410 nm was measured by UV-vis absorption spectroscopy.

Generation of •OH by the AHCu : Evaluate the •OH generation by a Cu^{2+}-catalyzed Fenton-like reaction is important. 60 $\mu g \bullet mL^{-1}$ of TMB, H_2O_2, $CuCl_2$, AHCu and AHCu + H_2O_2 (Cu^{2+} of 60 μM equiv) were incubated at 37 °C for 6 min. The generation of •OH was revealed by increasing absorption at 650 nm. (H_2O_2 concentration of 1 mM)

In vitro cytotoxicity study: Murine breast cancer cells(4T1), Human Umbilical Vein Endothelial Cells (HUVEC) were cultured in 96-well plates at 1×10^4 cells per well and incubated in 5% CO^2 at 37 ºC for 24 h. The cell viability was measured using the CCK-8 kit following the manufacturer's protocols. For cytotoxicity assessments, different concentrations of AH, AHCu, AH+H_2O_2 and AHCu+ H_2O_2 (100 μM equiv) were added. (H_2O_2 concentration of 50μM) After that, the cells were further incubated for 24 h. Then CCK-8 solution was added into each well and the absorbance of each well was detected at 450 nm using a microplate reader.

Live/dead cell staining assay: Fluorescein diacetate (FDA) and propidium iodide (PI) were used as stains to visualize the status of AHCu treated 4T1 cells. In brief, 4T1 cells were seeded in 6-well plate and cultured in the DMEM medium for 24 hours without any treatment. After co-cultured with H_2O_2, AH, AH+H_2O_2, AHCu and AHCu+ H_2O_2 (100 μM equiv) for 6 hours, the cells were co-stained with FDA and PI for 20 minutes, rinsed with PBS and observed using confocal microscopy. (H_2O_2 concentration of 50 μM)

Flow cytometry analysis: Apoptosis of 4T1 induced by AHCu+H_2O_2 was measured by flow cytometry using a FITC Annexin V Apoptosis Detection kit (BD, NJ, USA) according to the manufacturer's instrument. Typically, 4T1 cells were seeded in 12-well plates and incubated for 24 h. Then, the medium was replaced with DMEM containing H_2O_2, AH, AH+H_2O_2, AHCu, AHCu+ H_2O_2 (100 μM equiv) and further incubated for 24 h at 37 °C. After co-stained with Annexin-V FITC and PI, the cells were harvested and subjected for flow cytometry analysis. In each test, 15000 cells were analyzed. (H_2O_2 concentration of 50 μM)

Intracellular GSH depletion: 4T1 cells were seeded in 12-well plates. After treating with PBS, H_2O_2, AH, AH+H_2O_2, AHCu, AHCu+H_2O_2 for 6 h, the intracellular reduced glutathione (GSH) to oxidized glutathione (GSSG) were determined using a GSH and GSSG assay kit (Beyotime Institute of Biotechnology) according to the manufacturer's instructions. All the treatments were performed in triplicate in three independent experiments.

Intracellular ROS detection: The 2′,7′-dichlorofluorescin diacetate (DCFH-DA) was used for ROS detection in this study as described previous study. [2.3] 4T1 cells were seeded on Chambered cover glass (Lab-Tek Chambered 1.0 Borosilicate Cover Glass system, Nunc). After treating with PBS , H_2O_2 , AH, AH+H_2O_2, AHCu and AHCu + H_2O_2 for 6 h, the cellular ROS level was measured by ROS Assay Kit (DCFH-DA, Invitrogen TM). After the incubation, the cells were washed with PBS. Thereafter, ROS working solution (1 mL) was added. After washing out extra dyes, the cells were imaged under microscopy for observing the ROS level.

Animal model: Female Balb/c nude mice were purchased from Beijing Vital River Laboratory Animal Technology Co., Ltd. and used under protocols approved by Laboratory Animal Center in University of Science and Technology of China (USTC). To develop the tumor model, 1×10^6 4T1-Luc cells suspended in 100 μL Matrigel (Corning) were subcutaneously injected into the right back of each mouse. The mice were used when tumor volume reached about 60 mm^3 .

In vivo antitumor activity: The in vivo antitumor efficacy of AH and AHCu was performed in 4T1-Luc tumor bearing Balb/c mice. 4T1-Luc tumor mice were randomly allocated into 3 groups (n = 5): Group 1 - PBS (Control); Group 2 - AH:20 $mg\cdot kg^{-1}$; Group 3 - AHCu: 20 $mg\cdot kg^{-1}$ nanoprodrug. The mice were injected into tail vein on day 0, 2, 4 and 6 respectively. The tumor volume and body weight were measured every two days.

The IVIS imaging system was used to monitor tumor growth every 3 days. The tumor volume was calculated according to the equation: Volume = (Tumor length) × (Tumor width)^2/2 (mm^3). Relative tumor volume (V/V_0) was normalized to its initial size before administration. The body weights of all mice were recorded every other day during the treatment. At the end of the treatment (on the 16th day after the first administration), all mice were sacrificed and tumors were collected and weighted.

Pathological investigation: After in vivo therapy, tumor tissues of control, AH and AHCu groups were resected, fixed with 4% formaldehyde solution and embedded in paraffin blocks. The tissue blocks were sectioned and stained with hematoxylin and eosin (H&E). Terminal deoxynucleotidyl transferase (TdT)-mediated deoxyuridine triphosphate (dUTP) nick end labeling (TUNEL) staining was conducted using *in situ* BrdU-Red DNA Fragmentation Assay Kit (Abcam). All processes were carried out following the standard protocol

In vivo biocompatibility analysis： After in vivo therapy, the mice were euthanized and main organs (heart, kidney, liver, lung, and spleen) of the mice were harvested and fixed using 4% paraformaldehyde. Tissue samples were then embedded in paraffin, sliced (4 μm), and stained for further histological analysis by standard H&E staining procedure.

Statistical Analysis： Statistical analysis was perform using GraphPad Prism 8.0. All data were expressed as mean ± standard error of the mean. The statistical difference between

different groups of data was evaluated by one-way ANOVA, and $p < 0.05$ was considered to be statistically significant.

Supplementary Figures:

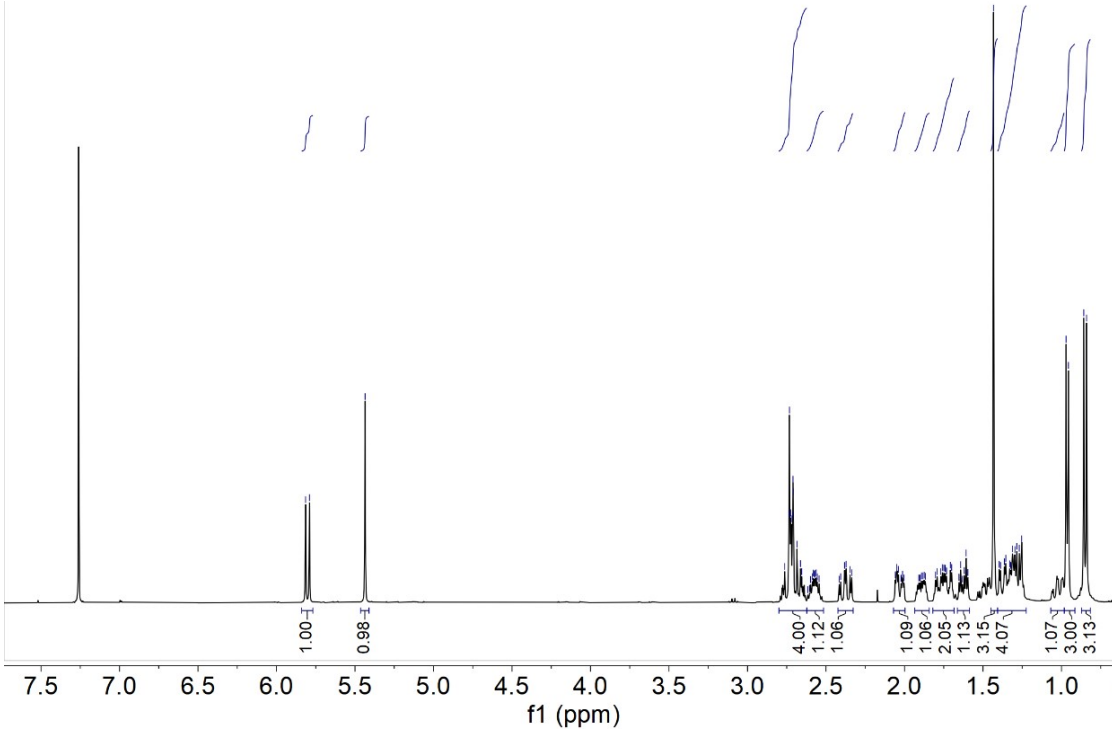

Figure S1. ^{1}H-NMR spectrum of Artesunate. ^{1}H NMR (400 MHz, Chloroform-*d*) δ 5.80 (d, *J* = 9.8 Hz, 1H), 5.44 (s, 1H), 2.81 – 2.63 (m, 4H), 2.62 – 2.50 (m, 1H), 2.38 (td, *J* = 14.0, 4.0 Hz, 1H), 2.03 (dt, *J* = 14.5, 3.8 Hz, 0H), 1.94 – 1.84 (m, 1H), 1.81 – 1.67 (m, 2H), 1.62 (dt, *J* = 13.8, 4.5 Hz, 1H), 1.43 (s, 3H), 1.41 – 1.22 (m, 4H), 0.96 (d, *J* = 5.9 Hz, 3H), 0.85 (d, *J* = 7.1 Hz, 3H).

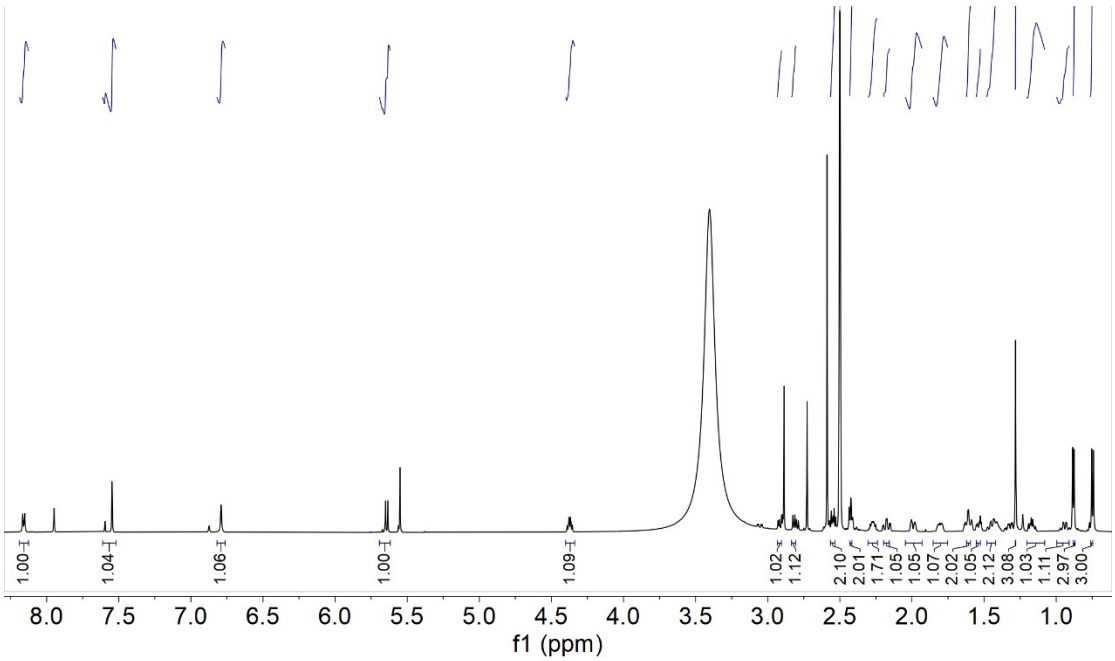

Figure S2. ^{1}H-NMR spectrum of AH. ^{1}H NMR (600 MHz, DMSO-d_6) δ 8.16 (d, J = 7.7 Hz, 1H), 7.57 (d, J = 29.4 Hz, 1H), 6.83 (d, J = 50.1 Hz, 1H), 5.64 (d, J = 9.8 Hz, 1H), 4.37 (td, J = 7.8, 5.4 Hz, 1H), 2.91 (dd, J = 14.8, 5.6 Hz, 1H), 2.81 (dd, J = 14.8, 8.0 Hz, 1H), 2.54 (dd, J = 11.8, 6.2 Hz, 1H), 2.42 (t, J = 6.9 Hz, 1H), 2.32 – 2.22 (m, 2H), 2.18 (td, J = 14.0, 3.9 Hz, 1H), 1.99 (dt, J = 14.6, 3.8 Hz, 1H), 1.81 (ddt, J = 13.6, 6.9, 3.6 Hz, 1H), 1.61 (td, J = 14.2, 13.7, 3.5 Hz, 2H), 1.53 (t, J = 4.4 Hz, 1H), 1.44 (dt, J = 13.0, 6.0 Hz, 1H), 1.28 (s, 3H), 1.17 (td, J = 11.4, 6.6 Hz, 1H), 1.01 – 0.90 (m, 1H), 0.88 (d, J = 6.4 Hz, 3H), 0.75 (d, J = 7.1 Hz, 3H).

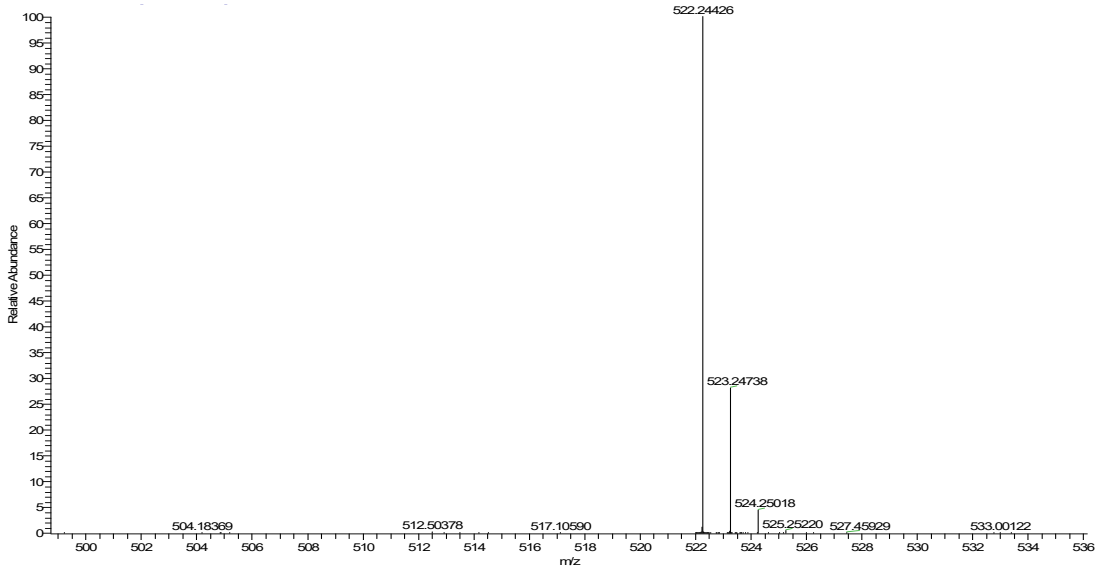

Figure S3. ESI-MS spectrum of AH ($[M + H]^+$). *m*/*z* calculated for $C_{25}H_{36}O_9N_3$($[M + H]^+$) 522.24426, found 522.24426.

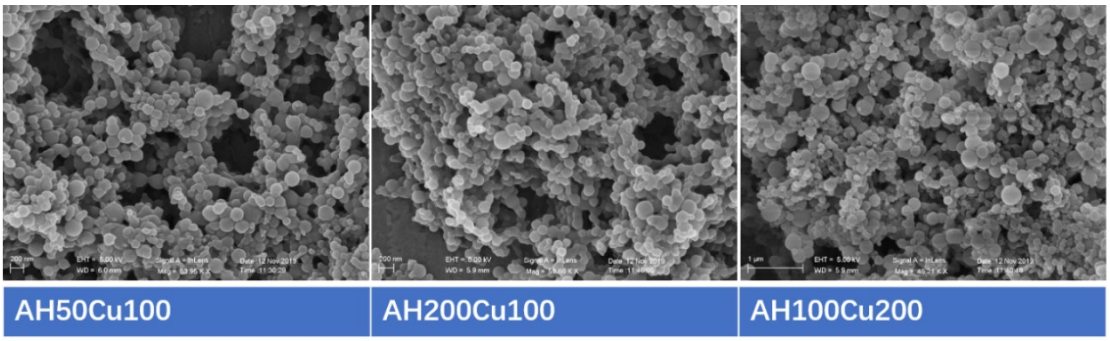

Figure S4. SEM images of AHCu at different feeding ratio of AH and Cu^{2+}. ((left: 1.9 mM AH; center: 7.6 mM AH; the Cu^{2+} concentration was fixed at 1 mM; right: 3.8 mM AH, the Cu^{2+} concentration was fixed at 2 mM).

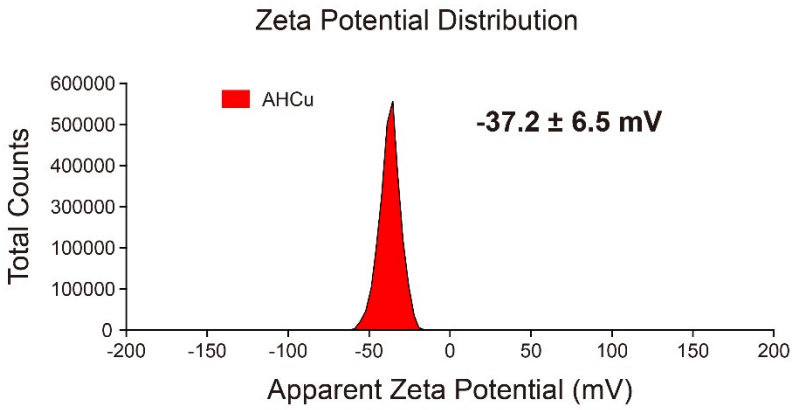

Figure S5. Zeta-potential distribution of AHCu nanoprodrug (pH = 7.4).

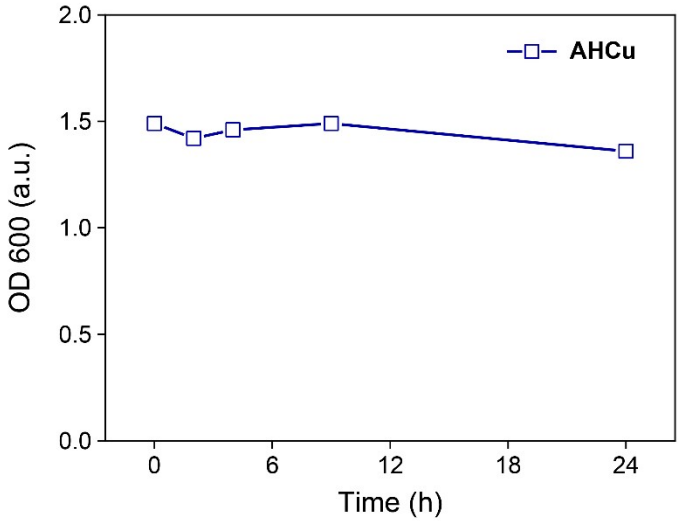

Figure S6. Turbidity monitoring (OD 600) of AHCu over 24 h.

Figure S7. Responsiveness of AHCu in the presence of GSH (left: AHCu; right: AHCu + 2mM GSH).

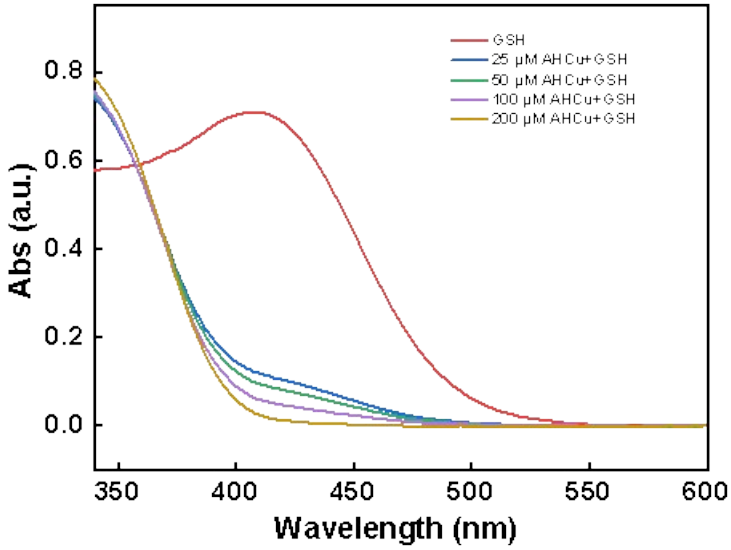

Figure S8. GSH depletion by different concentrations of AHCu.

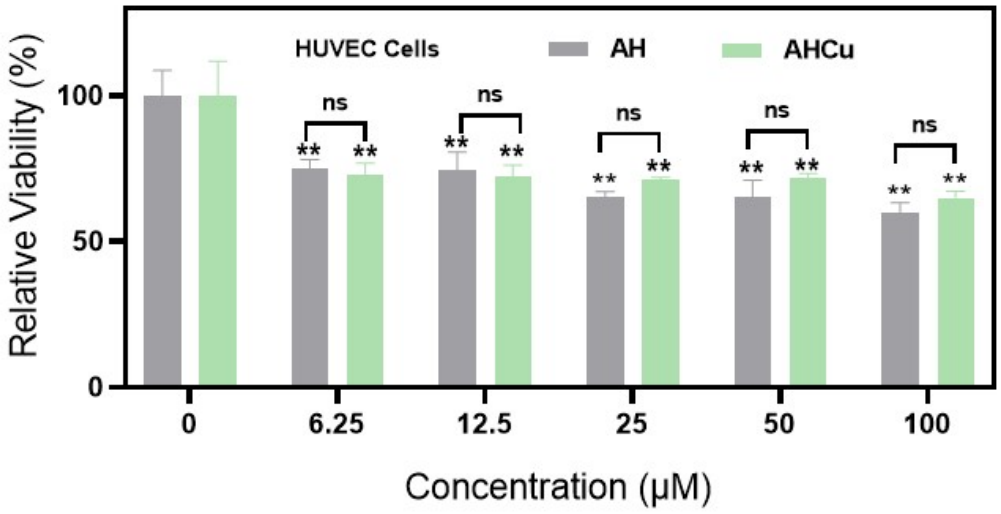

Figure S9. Cytotoxicity of AH and AHCu against HUVEC cells.

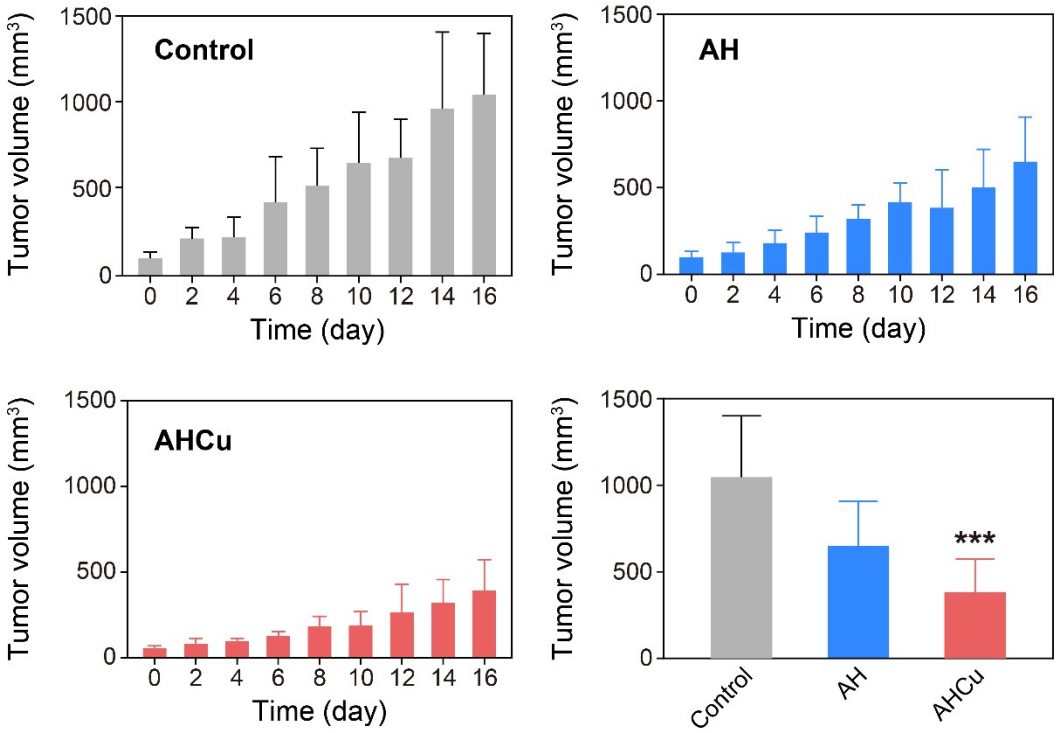

Figure S10. Tumor growth curves of different groups. Compared with control group, ***p<0.001. AH compared with AHCu group. $^{###}p$<0.001.

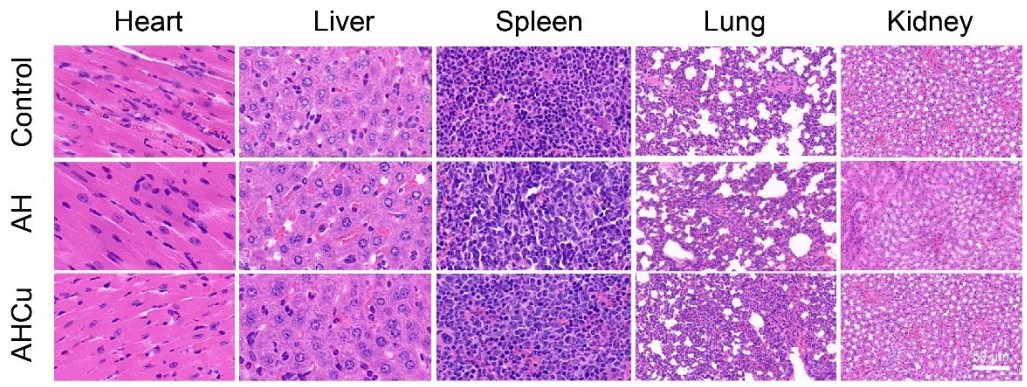

Figure S11. H&E staining of main organs (including heart, liver, spleen, lung and kidney) from Control, AH and AHCu group. No obvious abnormalities and inflammation in these tissues were observed.

Supplementary Table S1:

Batch No.	Cu^{2+} (ICP-AES)		AH (HPLC)		d.nm Z-Average	Loading content (w/w%)
	Feed (mM)	Detected (mM)	Feed (mg)	Detected (mg)		
1	1.0	0.95	1	0.83	236.2	68.5
2	1.0	0.91	2	0.75	165.6	68.1
3	1.0	0.89	3	0.50	143.3	66.4

Table S1. Drug loading efficiency at different AH/Cu feeding ratios. The concentrations of AH and Cu are detected by UPLC and ICP-AES, respectively.

Supplementary Table S2:

Table DLS_{AHCu}	Z-Average (d.nm)	PDI value
Batch 1	165.6 ± 0.5	0.162 ± 0.026
Batch 2	179.5 ± 0.7	0.153 ± 0.012
Batch 3	160.3 ± 0.8	0.141 ± 0.02

Table S2. Reproducibility of AHCu preparation at optimal AH/Cu feeding ratio. The hydrodynamic diameter and PDI profiles of independent batches of AHCu nanoprodrug are shown.

References:

[1]. P. Xu, X. Wang, T. Li, L. Li, H. Wu, J. Tu, R. Zhang, L. Zhang, Z. Guo, Q. Chen, *ACS Appl. Mater. Interfaces* **2021,** *13*, 33926-33936.

[2]. A. Aranda, L. Sequedo, L. Tolosa, G. Quintas, E. Burello, J. V. Castell, L. Gombau, *Toxicol. In Vitro* **2013,** *27*, 954-963.

[3]. M. Yazdani, *Toxicol. In Vitro* **2015,** *30*, 578-582.